The Indonesian Journal of Computer Science
www.ijcs.net
Volume 14, Issue 2, April 2025
https://doi.org/10.33022/ijcs.v14i2.4722

Enhancing Energy Generation Through Floating PV Integration with Existing Hydropower Station

Hnin Yu Wai[1], Wunna Swe[2], Swe Zin Oo[3]
hninyuwai2088@gmail.com[1], wunnaswe@mtu.edu.mm.com[2], swezinoo678@gmail.com[3]
[1,2,3] Department of Electrical Power Engineering, Mandalay Technological University, Mandalay, Myanmar

Article Information

Received : 10 Feb 2025
Revised : 7 Mar 2025
Accepted : 15 Apr 2025

Keywords

Floating Photovoltaic System, Kun Chaung Hydropower, Renewable Energy, Energy Output Analysis, Solar Irradiance.

Abstract

In this paper, the design and performance of an integrated floating photovoltaic (PV) system at the Kun Chaung Hydropower Station in Myanmar are analyzed. Hybridizing grid-connected hydropower with floating PV enhances renewable energy output. A site assessment evaluates the reservoir's suitability, considering solar irradiance, water levels, and environmental impacts. The proposed design includes PV module specifications, floating structures, and system integration. Energy output is analyzed under various conditions. Results show that the minimum hydropower generation in April, 24343 MWh, increases to 33865 MWh with floating PV, while maximum generation in November rises from 40878.2 MWh to 47768.6. Integration improves system capacity, ranging from 56.74 MW in May to 117.68 MW in October. These findings confirm the potential of floating PV to enhance energy generation. The study concludes with recommendations for implementation and highlights future research opportunities to optimize performance and assess economic feasibility.

A. Introduction

The growing demand for sustainable and efficient energy sources has led to innovative approaches in renewable energy integration. One of the emerging solutions is the development of floating solar photovoltaic (PV) systems, which are integrated with hydropower reservoirs to maximize energy production while minimizing environmental impacts. Floating solar PV systems have shown substantial potential in reducing land use, improving system efficiency, and generating additional energy from unused water surfaces. This technology has gained global attention as a promising alternative to conventional ground-mounted PV systems, particularly for countries where land scarcity is a concern [1,2].

Hydropower and solar energy are complementary in many ways, and their integration can significantly increase energy generation capacity. During peak sunlight hours, solar panels contribute to energy generation, while hydropower stations can supplement this energy during periods of reduced solar output. Such hybrid systems are not only beneficial in terms of energy diversification but also provide better grid stability and energy security [5, 26]. In addition, the cooling effect of water on floating solar panels enhances their performance by reducing the operating temperature of the PV modules. This cooling effect can lead to a notable increase in energy output, as high temperatures generally reduce the efficiency of PV panels [20, 26].

In recent years, floating solar systems, also known as photovoltaics, have been deployed in various parts of the world, especially in regions with large water bodies and significant solar potential. Research has shown that floating PV systems can increase power generation efficiency by 10-15% compared to land-based systems due to lower temperatures and reduced dust accumulation [2, 20]. Moreover, by utilizing existing reservoirs, floating solar projects avoid the environmental and social impacts associated with land acquisition and deforestation, making them a more environmentally friendly option for solar power deployment [3, 25].

The Kun Chaung Dam, located at 18° 29' N latitude and 96° 26' E longitude in the Bago region, is a prime location for implementing this innovative energy solution. The dam's large reservoir offers a suitable surface for installing a floating solar system, which can work in tandem with the existing hydropower infrastructure to create a reliable and efficient hybrid energy system [17]. Studies have highlighted the importance of optimizing the tilt angle and orientation of PV panels to achieve maximum solar energy capture, with tilt angles varying according to the location and time of year [9, 15]. For the Kun Chaung site, calculations and simulations are essential to determine the optimal tilt angle and orientation that maximize energy output throughout the year.

This research explores the design and performance analysis of a floating solar PV system integrated with hydropower at the Kun Chaung reservoir. The study involves detailed modeling and simulation of the floating PV system, considering critical factors such as solar irradiation, temperature, wind velocity, and azimuth angles. It also compares the performance of the floating system with traditional ground-mounted PV systems, emphasizing the benefits of reduced thermal losses and the synergies between solar and hydropower generation [8, 26]. The integration of floating solar with hydropower not only enhances the overall energy yield but also contributes to grid stability and supports Myanmar's transition towards a more sustainable and resilient energy system [5, 17]. Additionally, the research incorporates data from reliable sources, such as NASA Surface Meteorology and Solar Energy, to simulate solar radiation and temperature profiles, ensuring accurate performance analysis [19].

By conducting this comprehensive study, the paper aims to provide valuable insights into the potential of floating solar PV systems in Myanmar and promote their adoption in similar regions worldwide. The findings will contribute to the understanding of renewable energy integration and support policymakers and engineers in designing efficient and sustainable energy systems [23].

B. Methodology

The methodology for this study involves the design and analysis of a 30 MW floating solar photovoltaic (PV) system integrated with the existing hydropower infrastructure at the Kun Chaung Dam. A detailed assessment of the dam's site characteristics, including the reservoir area, geographical location, and hydropower capacity, is conducted to determine the feasibility of solar integration. The SG1100UD centralized inverter is selected for its suitability, and its operational characteristics are analyzed. Key performance indicators, including module temperature, irradiance, and wind velocity, are examined to evaluate system efficiency. The energy output and overall performance of the integrated system are assessed under various environmental conditions. The results are compared with those of traditional energy systems to determine the benefits of the integrated solar-hydropower approach.

1. Case Study Area

The Kun Chaung Dam, located in Myanmar's Bago region, presents a promising case for integrating floating solar PV technology with its existing hydropower infrastructure. The dam is situated on the Kun Chaung River, and its reservoir, which covers approximately 10.03 million square meters, makes it ideal for solar energy generation. By harnessing solar power alongside hydropower, the Kun Chaung Dam can enhance regional energy security, reduce reliance on traditional energy sources, and contribute to environmental sustainability. This integration also offers additional benefits, such as water evaporation reduction and efficient use of space, accelerating Myanmar's transition to a more resilient and sustainable energy future.

The Kun Chaung Dam is located on a tributary of the Si Taung River, approximately 9 miles southwest of Phyu City. The reservoir's water surface area is estimated at approximately 10.0328×10^6 square meters and is situated at 18° 29′ N latitude and 96° 26′ E longitude. The proposed floating PV system is designed to be installed on the reservoir surface, as shown in Figure 1. The dam's location and expansive water surface provide an ideal setting for floating PV deployment, reducing land use conflicts while enhancing energy generation efficiency. By leveraging the untapped solar potential of reservoirs like the Kun Chaung Dam, the transition towards a sustainable and resilient energy future can be accelerated while unlocking new opportunities for water resource management and ecosystem.

Figure 1. Location map of the surface of Kun Chaung Dam

2. Floating Solar PV Plant Design

The design process for a Floating Solar Photovoltaic (FSPV) system integrated with hydropower at Kun Chaung starts with a comprehensive assessment of the reservoir's available surface area. This initial evaluation is critical, as it determines the potential size and capacity of the FSPV system. Following this, the design incorporates several key components, including:

- Anchoring and mooring system
- Floating platform
- PV modules
- Inverters
- Tilt Angle Calculation

Figure 2. Installed PV System Area on Kun Chaung Dam

Specific considerations related to the facility must be considered when designing the Floating Solar Photovoltaic (FSPV) plant for the Kun Chaung Dam in Bago. For the simulation, the FSPV's total capacity is set at 30 MW, corresponding to a dam area of approximately 167976 square meters. Fig. 2 illustrates the dimensions of the FSPV.

Designing the Floating Solar PV system is quite similar to designing a regular solar PV system but with adjustments made specifically for floating it on water. A standard floating framework provides support for the PV system, accommodating the arrays, inverters, combiner boxes, and other essential components [21]. These components are mounted on a single platform, with the bed typically constructed of materials such as fiber-reinforced plastic and floats (FRP), metal structures, or high-density polyethylene (HDPE).

2.1. Anchoring and Mooring System

The mooring and anchoring system is a critical component of a floating solar PV installation, responsible for securing the floating platform in place on the water's surface. This system typically consists of anchors, mooring lines, cables, ropes, or chains that connect the floating structure to fixed anchor points on the bottom of the water body or stable structures such as shorelines or buoys. It plays a crucial role in preventing drift and maintaining the position of the solar array, ensuring stability and functionality even in the face of external forces such as wind, waves, and currents [12]. Other font types may be used if needed for special purposes.

2.2. Floating Platform

The floating platform, also known as a pontoon, is typically constructed from a series of high-grade plastic fiber floats securely bound together. This platform is a robust foundation for supporting solar panels atop water bodies.

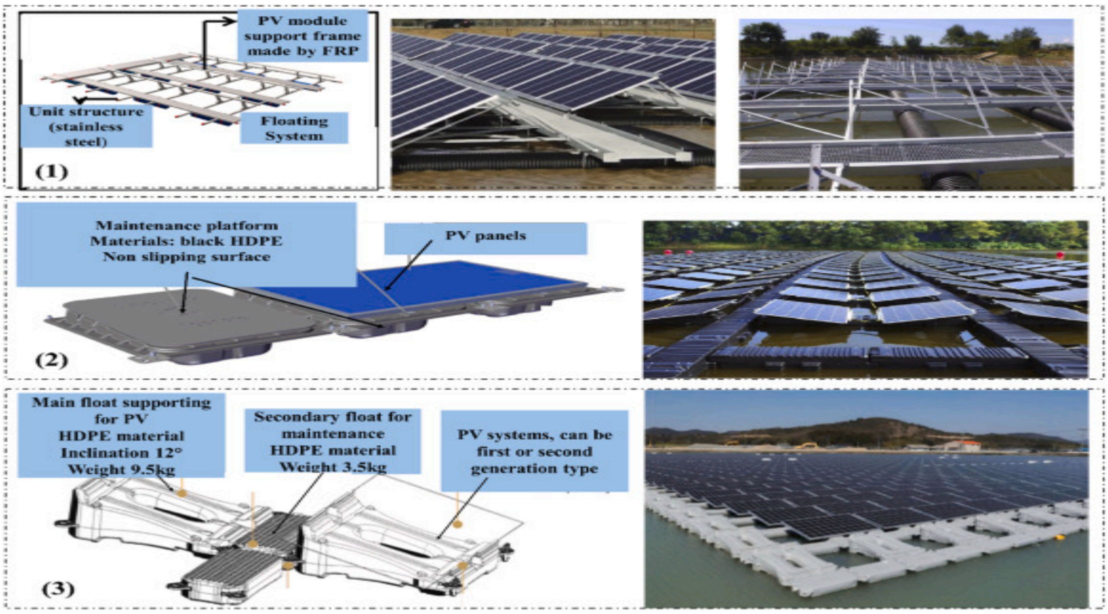

Figure 3. Different types of structures are employed for FPV application [2]

While the floating platform possesses considerable strength, its inherent buoyancy allows it to move freely with water currents. However, given the significant capacity of the hydropower reservoir and the potential impact of flows and waves, the float system alone cannot withstand the forces exerted by large PV arrays. Thus, a floating bridge system is essential to anchor the arrays securely against wave, wind, and flow effects. The typical structure design of a floating solar with an anchoring system is shown in Figure 3.

The floating structure comprises shaped HDPE plastic material with dimensions of 507 × 507 × 400 mm, a 3 mm thickness with reinforced ribs, and a load-bearing capacity of 95 kg per float. With a product lifespan exceeding 25 years, the floating bridge measures 3.0 meters in width, ensuring stability and durability for the installed PV arrays.

2.3. Meteorological Parameters and Floating PV Cell Temperature

The temperature of floating photovoltaic (PV) cells is influenced by various factors, including solar radiation intensity, ambient temperature, wind speed, and water temperature. Generally, floating PV systems experience lower cell temperatures compared to traditional land-based PV systems due to the cooling effect of water beneath them. The average solar radiation in Table 1, the minimum and maximum ambient daily temperature in Table 2, and the average wind speed in Table 3 for the last 20 years are presented.

Table 1. Monthly Averaged Insolation Incidents on A Horizontal Surface (kWh/m2/day)

Lat 18 / Lon 96	Jan	Feb	Mar	Apr	May	Jun	Jul	Aug	Sep	Oct	Nov	Dec	Annual Average
22-year Average	5.24	5.95	6.43	6.6	5.49	4.04	3.91	3.79	4.47	4.76	4.76	4.91	5.03

Table 2. Monthly Averaged Air Temperature at The Surface Of The Earth (°C)

Lat 18 Lon 96	Jan	Feb	Mar	Apr	May	Jun	Jul	Aug	Sep	Oct	Nov	Dec	Annual Average
22-year Average	22.5	24.6	27.3	29	27.2	25.6	25.2	25.1	25	24.6	23.3	22	25.1
Minimum	17	18.3	21.1	24.3	24.2	23.4	23	22.8	22.6	21.9	19.9	17.7	21.3
Maximum	28.2	30.1	32.3	33.2	30.2	27.8	27.6	27.8	28	28.1	27.4	27	29

Table 3. Monthly Average Wind Speed at The Surface of The Earth (m/s)

Lat 18	Jan	Feb	Mar	Apr	May	Jun	Jul	Aug	Sep	Oct	Nov	Dec	Annual

Lon 96													Average
10-year Average	3.19	3.49	3.43	3.01	2.69	3.45	3.39	3.16	2.52	2.52	2.96	3.12	3.07

The temperature of floating PV cells is affected by solar radiation, ambient temperature, wind speed, and water temperature. Cooling from water generally reduces cell temperatures compared to land-based systems.
Cell temperature on land is given by

$$T_{cl} = 0.943T_a + 0.0195G - 1.528V_{wL} + 0.3529 \quad (1)$$

Where,

$T_{cl} -$ cell temperature on land

$T_a -$ Ambient temperature(°C)

$G -$ Standard test conditions (STC) irradiation $\left(\frac{1000W}{m^2}\right)$

$v_{wL} -$ land wind speed

Cell temperature on water is given by

$$T_{cw} = 0.943T_w + 0.0195G - 1.528V_{ww} + 0.3529 \quad (2)$$

$$T_w = 5 + 0.75\,T_a \quad (3)$$

$T_w -$ *water temperature* (°C)

$V_{ww} -$ water wind speed

$$V_{ww}=1.62+1.17v_{wL} \quad (4)$$

$$T_{fpv} = 1.8081 + 0.9282.T_a + 0.0221.G - 1.2210.V_{w,w} + 0.0246T_{cw} \quad (5)$$

$T_{fpv} -$ floating cell temperature(°C)

The monthly variations in ambient temperature and the operating temperature of the floating PV system are presented in Table 4 and the graph, highlighting its thermal performance throughout the year.

Table 4. Temperature Differences Between Floating and Land-Based PV Systems

Month	T_a	$V_{w\ land}$	T_w	T_{cl}	T_{cw}
1	28.2	3.19	21.65	41.57	35.39
2	30.1	3.49	23.08	42.90	36.28
3	32.3	3.43	24.73	45.07	37.93
4	33.2	3.01	25.40	46.56	39.21
5	30.2	2.69	23.15	44.22	37.57
6	27.8	3.45	21.35	40.80	34.71
7	27.6	3.39	21.20	40.70	34.66
8	27.8	3.16	21.35	41.24	35.16
9	28	2.52	21.50	42.41	36.28
10	28.1	2.52	21.58	42.50	36.35
11	27.4	2.96	21.05	41.17	35.18
12	27	3.12	20.75	40.55	34.65

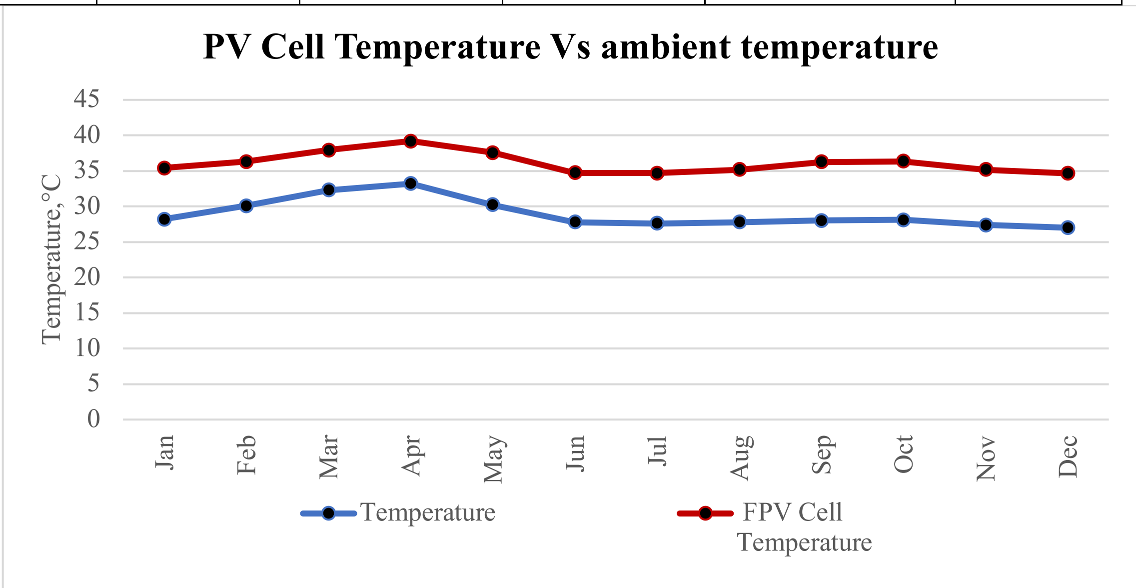

Figure 4. Comparison of Cell Temperature: Land-Based PV, Floating PV, and Ambient Temperature

2.4. Sizing of PV System

The proposed systems have Thirty PV arrays and the capacity of each PV array is 1 MWP. In this research, the capacity of PV source is 30 MW and the LONGI, LR5-72HBD 535~555W module type is used for PV array. Table 5. shows the characteristics of this module.

Table.5. Characteristics of Module

No	Parameters	Rating
1	Module Power	550 W
2	Voltage at Maximum power	41.95 V
3	Current at maximum power	13.12 A
4	Short-circuit current (I_{sc})	13.99 A
5	Open-circuit voltage (V_{oc})	49.8 V
6	Cells per module	144 cells

$$V_{Dc\ Link} = 2\sqrt{2}V_{rms} \tag{6}$$
$$= 2\sqrt{2} \times 400 = 1131.37 \sim 1150\ V$$

Firstly, the string voltage of an array is considered 1150 V. After choosing the string voltage, the number of modules in a string is given by,

$$\text{Numbers of Modules } (N_m) = \frac{\text{String Voltage } (V_{\text{string}})}{\text{Voltage at Maximum Power Point } (V_{\text{mpp}})} \tag{7}$$

$$\text{Numbers of Modules } (N_m) = \frac{1150}{41.95} = 27.4 \cong 28\ Modules\ per\ String$$

And, the string power is,

$$\text{String Power } (P_{\text{string}}) = N_m \times P_{\text{mpp}} \tag{8}$$

$$\text{String Power } (P_{\text{string}}) = 28 \times 550 = 15.4kW$$

where; N_m is the number of modules per string and P_{mpp} is the maximum power produced by a module.

If the array power is taken as approximately 1 MW, the number of strings in an array is given by,

$$\text{Number of strings in an array } (N_{\text{string}}) = \frac{P_{\text{array}}}{P_{\text{string}}} \tag{9}$$

$$\text{Number of strings in an array } (N_{\text{string}}) = \frac{1 \times 10^6}{15.4 \times 10^3} = 64.5 \sim 6\ 5 = 65\ strings$$

where, P_{array} is array power.

Total number of modules for each 1MW Central Inverter (N_T);

$$\text{Total number of modules } (N_T) = N_m \times N_{\text{string}} \tag{10}$$

$$\text{Total number of modules } (N_T) = 28 \times 65 = 1820\ modules$$

Number of arrays for a total 30MW power generation can be calculated as,

$$N_{\text{array}} = \frac{P_{\text{total array}}}{P_{\text{array}}} \tag{11}$$

$$N_{\text{array}} = \frac{P_{\text{total array}}}{P_{\text{array}}} = \frac{30 \times 10^6}{1 \times 10^6} = 30\ arrays$$

where, N_{array} is number of arrays and $P_{\text{total array}}$ is power output from total array.

The total number of modules for the system is given by,

$$N_{T,Sys} = N_m \times N_{\text{string}} \times N_{\text{array}} \tag{12}$$

$N_{T,Sys} = 28 \times 65 \times 30$ = 54600 modules

Where $N_{T,Sys}$ is total number of modules for the system.

Number of Strings for Each Combiner Box, $N_{Cbox,String}$;

$$N_{Cbox,String} = \frac{Number\ of\ Strings\ in\ each\ 1\text{MW}\ Inverter}{Number\ of\ Combiner\ \text{box}\ in\ an\ Inverter} \quad (13)$$

$$N_{Cbox,String} = \frac{65}{5} = 13\ Strings$$

Number of PV Modules for each Combiner Box, N_{Cbox} ;

N_{Cbox} = Numbers of Modules, N_m × Number ofString in any Array, N_{string} (14)

$$N_{Cbox} = 28 \times 13 = 364\ Modules$$

Number of PV Modules for each 1MW Inverter = Five Units of Combiner Boxes = 5×364 = 1820 Modules

Number of modules for each box Transformer, $N_{T,\ array}$ = Six Units of 1MW Inverter

$N_{T,\ array}$ = 6 × (5 × 364) = 10920 Modules

The total number of modules for total power generation can be calculated as,

N_T = Number of Transformer × Number of Modules for each box Transformer, $N_{T,array}$ (15)

$$N_T = 5 \times 10920 = 54600 Modules$$

The total rated power generation of the system,

P_T = N_{array} × the capacity of each rated Power, PV array (16)

P_T = 30 × 1MW = 30MW

The 54600 Pieces of LONGI bifacial mono-crystalline silicon solar PV modules (peak power 550W), and 30 sets of 1MW Central Inverter Station will be used in this system. Each string is composed of 28 modules, a total of 1950 strings, the total installed capacity on the system is 30MW, and the installed capacity on the DC side is 30.03MW, it consists of 5 groups of 6 MW PV arrays. All areas of the square array are equipped with 13 strings of 550W modules and 150 combiner boxes, of which 30 are connected to 13 strings. The five PV arrays are connected to the 33kV side of the newly built 33kV switchyard in two 33kV collecting Lines. A schematic diagram of the 30MW Floating PV plant is shown in Fig. 5.

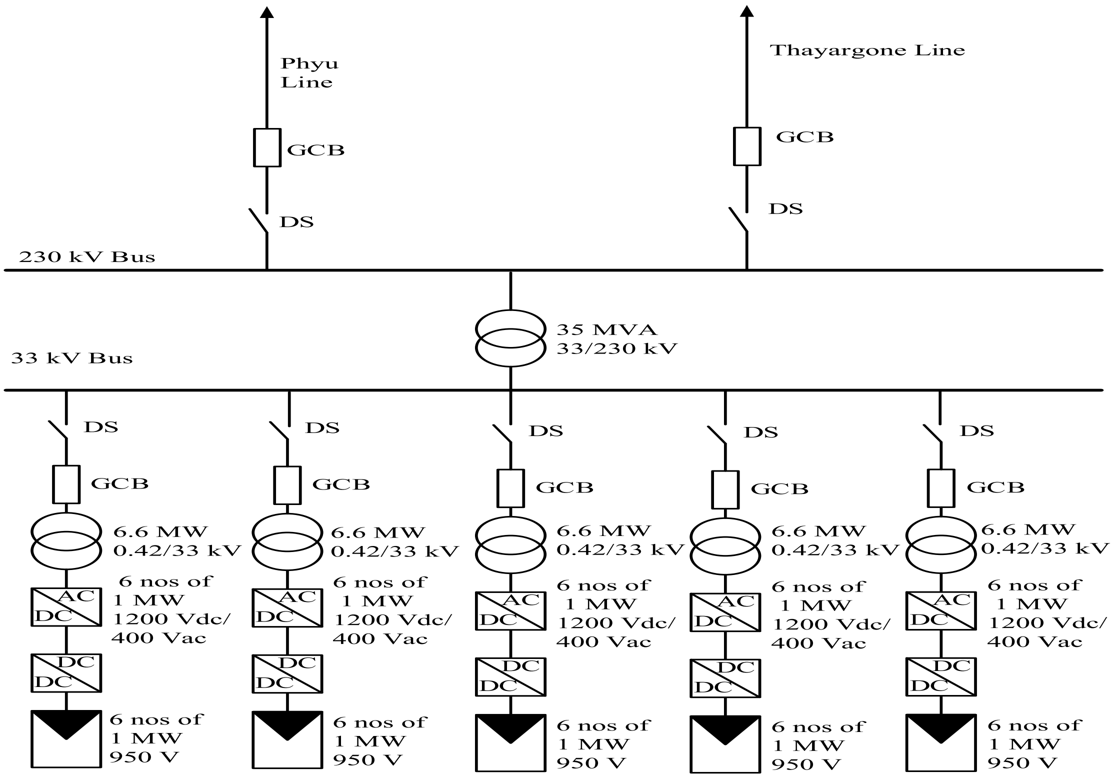

Figure 5. Single Line Diagram of 30 MW FPV Plant

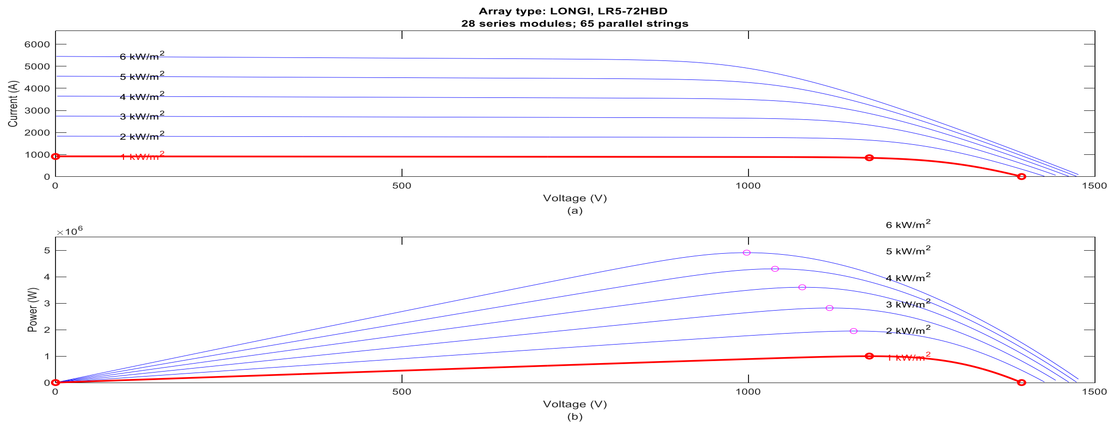

Figure 6. (a). V-I characteristic curve, (b) V-P characteristic curve of PV array at different irradiance

The curve in figure 6 demonstrates the effect of solar radiation on power output. As irradiance increases, the power output rises proportionally, reflecting the system's dependence on sunlight intensity. Simulations are conducted for each 1 MW inverter unit to assess performance under varying irradiance conditions.

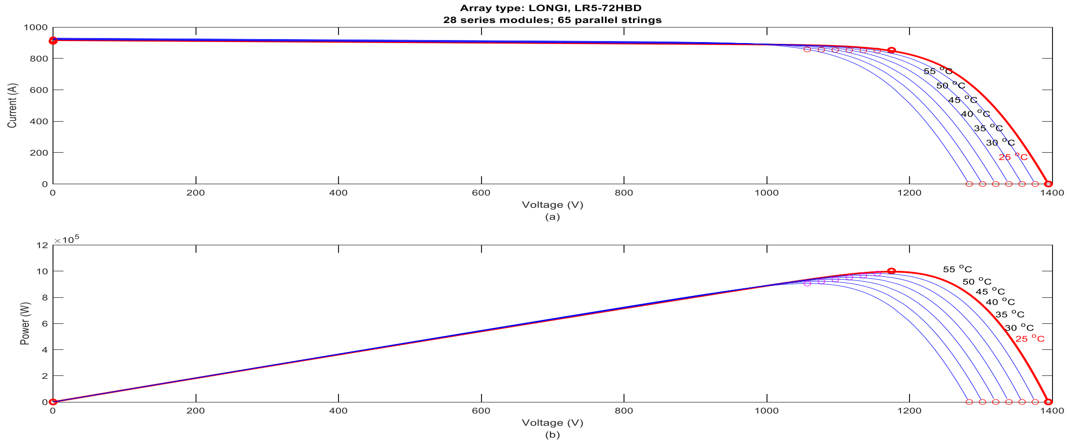

Figure 7. (a) V-I characteristic curve, (b) V-P characteristic curve of PV array at different temperature

The curve in figure 7 shows the relationship between temperature and power output. As the temperature rises, a gradual decrease in power output is observed. Simulations are performed for each 1 MW inverter unit to analyze the performance of the floating PV system under varying thermal conditions.

The daily energy output from the PV array can be calculated as follows:

$$E_{PV} = W_P \left(f_{\frac{dc}{ac}}\right)\left(\frac{G}{G_{STC}}\right)\left[1 + \beta(T_c - T_{STC})\right] \quad (17)$$

G_{STC} – Solar radiation incident under STC of [1000W/m2]

G – Soalr radiation incident on PV array in [kW/m^2]

$f_{\frac{dc}{ac}}$ – DC to AC derating factor [%] = 0.778

Wp – Rated capacity of PV array in [kWor watts], meaning power output under (STC)

G – Soalr radiation incident on PV array in [kW/m^2]

β – temperature coefficient of power (%/°C)

T_c – PV cell temperature in current time step(°C)

T_{STC} - nperature under STC(25°C)

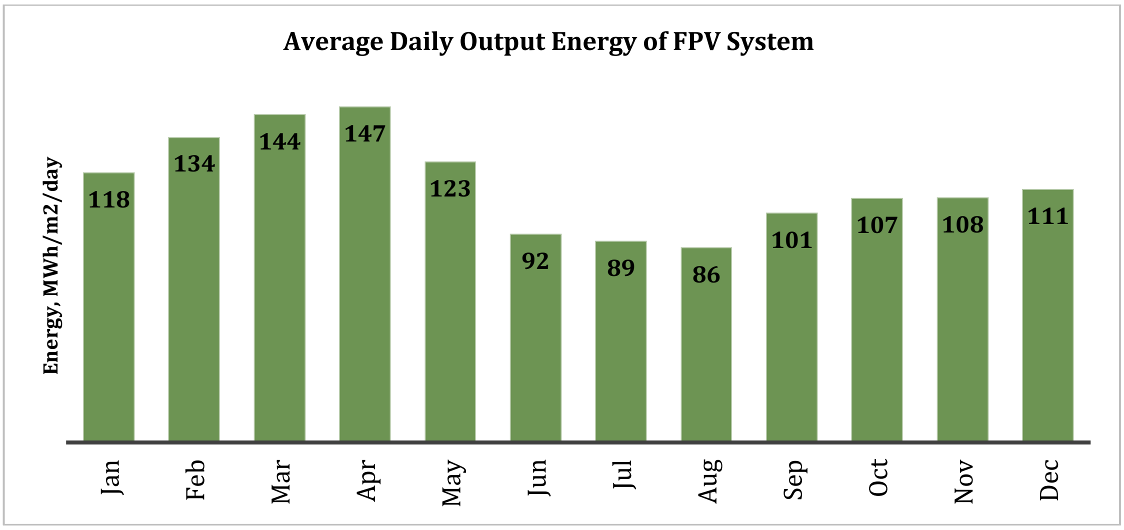

Figure 8. Average Daily Energy of FPV System

In Figure 8, the calculated daily energy output of the floating PV system is presented, showing their performance throughout the analysis period.

2.5. Sizing of Inverter

The sizing of the inverter for the floating PV array involves selecting inverters capable of converting the direct current (DC) generated by the solar panels into alternating current (AC) for grid integration. In this system, 30 inverters, each rated at 1 MW, are used to match the total DC output of the PV array while meeting efficiency and reliability requirements. The sizing process considers factors such as system voltage, grid compatibility, and future scalability, with a safety factor of 1.25 applied to accommodate potential expansions and ensure operational reliability.

$$P_{inv} = P_{max}\, 1.25 = 1.25MW$$

P_{inv} - Inverter power

P_{max} - Maximum power

$$\text{selected } P_{inv} \text{ rating} = \frac{\text{Rating } P_{inv}}{\text{efficiency}} = \frac{1.25M}{99\%} = 1.26 \text{ MW}$$

The inverter to be used for this system should have capacity not less than 1.26 MW. SG1100UD-20 inverter with maximum efficiency of 99% is selected for this design.

Table 6. Inverter specifications

Module	SG1100UD-20
Maximum power output	1320 kVA
Maximum DC input voltage	1500V
Minimum input DC voltage	938V
Nominal AC voltage	660V

THD%	<3%
Maximum efficiency (%)	99%

2.6. Tilt Angle Calculation

As part of the design and integration of the floating solar PV (FPV) system with the existing hydropower plant (HPP) at Kun Chaung Dam, determining the optimal tilt angle and orientation was critical to maximize energy capture and ensure seamless hybrid operation. The tilt angle directly impacts the solar radiation absorbed by the PV modules, while the azimuth angle influences their alignment with the sun's trajectory. To achieve the best configuration, an extensive analysis was conducted using solar radiation data. In table 7, the variation in solar irradiation is presented across tilt angles from 0° to 90°, providing a broad overview of energy potential. Table 8 narrows the focus to tilt angles between 15° and 25°, pinpointing the most effective range for optimization. This detailed evaluation confirmed that a tilt angle of 22° delivers the highest energy capture for the site.

Table 7. Solar Radiation Values for Tilt Angles Between 0° and 90°

	H^{β}_{month} kWh/m2*month										
Month/β	0	10	20	30	40	50	60	70	80	90	Max
1	162.44	183.21	199.31	210.25	215.69	215.47	209.60	198.25	181.77		215.69
2	166.60	180.15	189.15	193.34	192.58	186.91	176.49	161.63	142.80	120.56	193.34
3	199.33	205.81	207.25	203.60	194.98	181.64	163.99	142.57	118.02	91.11	207.25
4	198.00	195.59	188.67	177.46	162.32	143.72	122.31	98.89	74.54	51.24	198.00
5	170.19	163.89	154.37	141.90	126.89	109.87	91.53	72.79	55.20		170.19
6	121.20	116.59	110.02	101.67	91.81	80.82	69.14	57.44	46.91		121.20
7	121.21	117.52	111.77	104.14	94.87	84.28	72.79	60.96	49.71		121.21
8	117.49	116.27	112.85	107.33	99.88	90.74	80.22	68.70	56.68	45.04	117.49
9	134.10	137.25	137.44	134.67	129.03	120.67	109.87	96.93	82.27	66.32	137.44
10	147.56	157.90	164.55	167.31	166.11	160.97	152.06	139.63	124.08	105.87	167.31
11	142.80	159.79	172.88	181.69	185.93	185.49	180.37	170.73	156.87		185.93
12	152.21	174.48	192.33	205.22	212.75	214.71	211.03	201.82	187.36		214.71
Year	1833.13	1908.44	1940.59	1928.58	1872.83	1775.28	1639.38	1470.35	1276.21	480.15	1940.59

Table 8. Solar Radiation Values for Tilt Angles Between 15° and 25°

	H^{β}_{month} kWh/m2.month										
Month β	15	16	17	18	19	21	22	23	24	25	Max
1	191.88	193.47	195.00	196.49	197.93	200.64	201.92	203.15	204.33	205.45	205.00
2	185.24	186.11	186.94	187.73	188.46	189.79	190.38	190.92	191.41	191.86	192.00
3	207.17	207.29	207.35	207.37	207.33	207.11	206.93	206.69	206.40	206.06	207.00
4	192.68	191.97	191.21	190.41	189.56	187.74	186.77	185.75	184.69	183.59	193.00
5	159.52	158.55	157.55	156.52	155.46	153.25	152.10	150.92	149.72	148.48	160.00
6	113.54	112.87	112.19	111.48	110.76	109.26	108.48	107.69	106.88	106.05	114.00
7	114.89	114.31	113.70	113.08	112.44	111.09	110.39	109.67	108.93	108.18	115.00
8	114.83	114.48	114.10	113.71	113.29	112.39	111.91	111.41	110.88	110.34	115.00
9	137.72	137.72	137.70	137.64	137.56	137.30	137.12	136.92	136.69	136.43	138.00
10	161.70	162.34	162.95	163.52	164.06	165.00	165.42	165.79	166.13	166.42	166.00
11	166.85	168.14	169.39	170.60	171.76	173.96	175.00	175.99	176.94	177.84	178.00
12	183.99	185.76	187.47	189.14	190.76	193.85	195.32	196.74	198.10	199.42	199.00
Year	1930.01	1933.01	1935.57	1937.69	1937.36	1941.38	1941.73	1941.63	1941.10	1940.11	1941.73

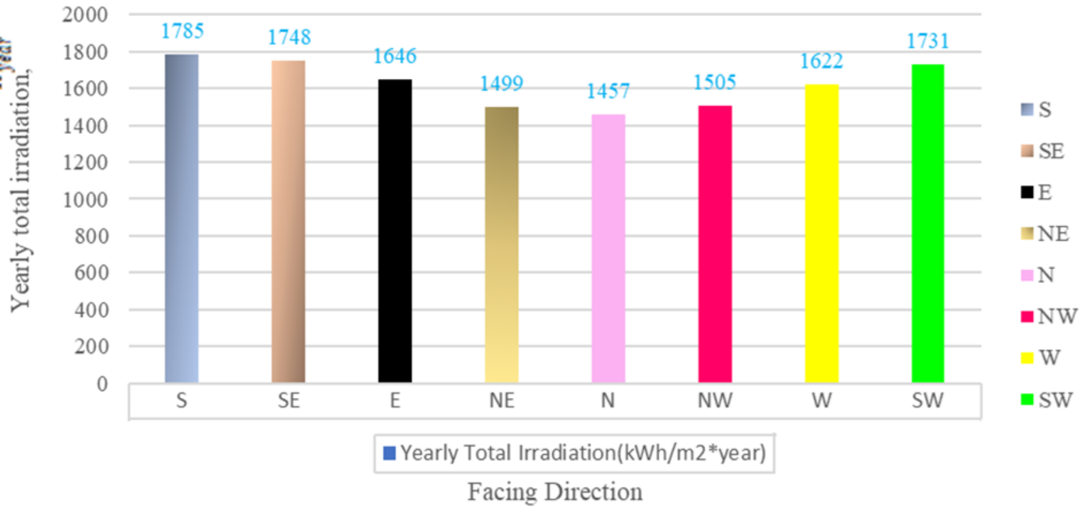

Figure 9. Comparison of Total Irritation at Different Azimuth Angle

Additionally, in figure 9, solar irradiation at different azimuth angles is examined, emphasizing the importance of southward orientation for maximizing energy yield at the Kun Chaung Dam's latitude (18° 29' N). Incorporating these optimized angles into the FPV system design ensures efficient energy production, which complements the existing hydropower system. The hybrid operation leverages the strengths of both technologies, with the FPV system mitigating seasonal hydropower variability and enhancing the overall reliability of energy generation. This integrated approach exemplifies the benefits of combining FPV with HPP for sustainable, efficient, and land-conserving energy solutions.

C. Evaluation of the Integrated PV System

This section focuses on assessing the performance of the integrated photovoltaic (PV) system based on key parameters such as solar irradiance, module temperature, and tilt angle. The system's design and operational characteristics are analyzed to determine its efficiency and energy output under varying environmental conditions. A schematic representation of the integration and interactions among components is provided in Figure 10. The evaluation highlights the system's response to changing input conditions and identifies potential areas for optimization. Additionally, the findings are compared with theoretical expectations to ensure the reliability and effectiveness of the integrated PV system.

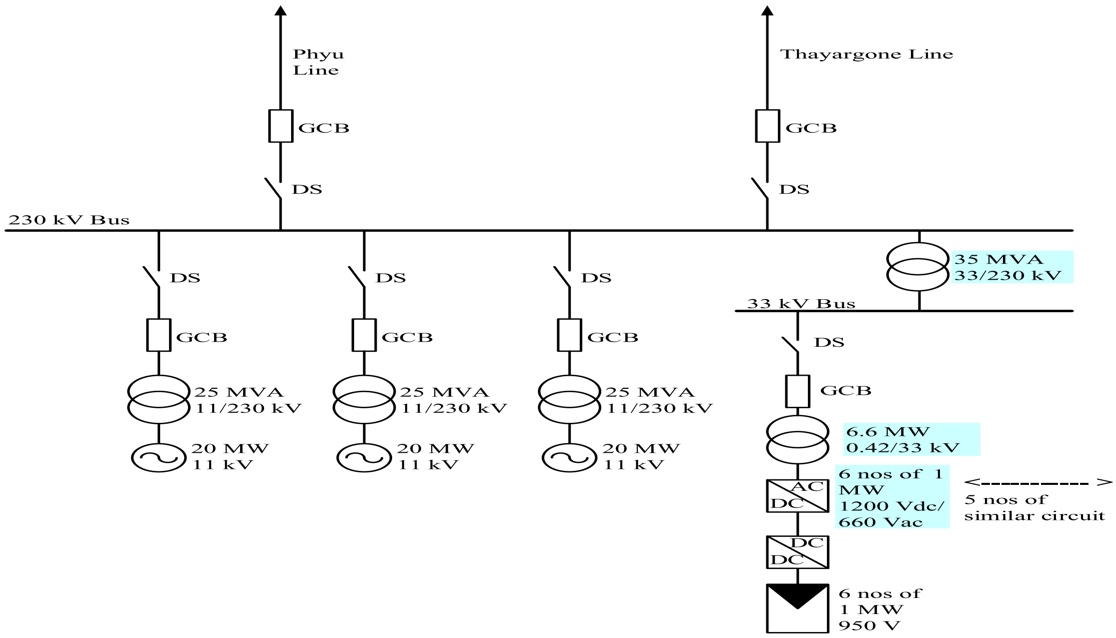

Figure 10. Desired the Single Line Diagram for a Simulink Model of Integrated floating PV system

Table 9. Hydro Power Generation for each Month

Months	Rainfall (mm)	H(m)	Discharge, Q (m3 /sec)	Evapouration rate (m 3 /sec)	Power, P (MW)	Power (p.u)	Energy, E (MWh)
Jan	2.7	160.099	30.2949	3.77	47.59	0.79	34261.68
Feb	2.5	159.797	29.3189	4.33	45.97	0.77	33097.68
Mar	9.4	158.914	27.0448	6.77	42.17	0.70	31372.88
Apr	23.8	157.188	23.4840	6.09	36.22	0.60	24343
May	103.3	155.911	18.5449	2.95	28.37	0.47	21105.48
Jun	160.1	156.152	23.4701	0.76	35.96	0.60	26751.47
July	180.8	157.17	25.9897	0.74	40.08	0.67	29817.48
August	187.5	159.42	27.8412	0.85	43.55	0.73	32403.36
Sept	132.4	161.032	31.9168	0.96	50.43	0.84	37523.49
Oct	70.1	161.568	35.2487	0.88	55.88	0.93	40231.84
Nov	22.2	161.34	34.7048	0.88	54.94	0.92	40878.2
Dec	6.1	160.243	30.5157	1.95	47.98	0.80	35697.64

Hydropower generation is shown in Table 9 and Figure 11, where the highest output is recorded in August due to peak water levels during the rainy season. In contrast, the lowest generation is observed in February, reflecting reduced water availability in the dry season. The generation is also commanded by demand from the load control center, highlighting the role of seasonal dependency and load requirements in hydropower production. Additionally, Figures 8 indicates that for floating PV systems, April has the highest energy output, while August records the lowest, highlighting the impact of seasonal factors on energy generation.

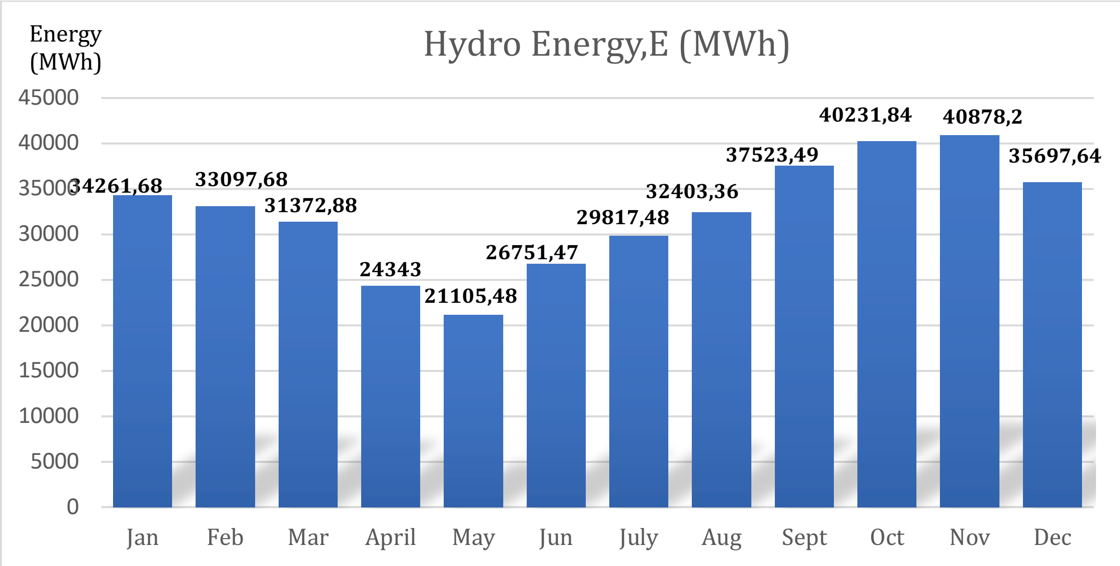

Figure 11. Hydro Power Energy Generation for each Month

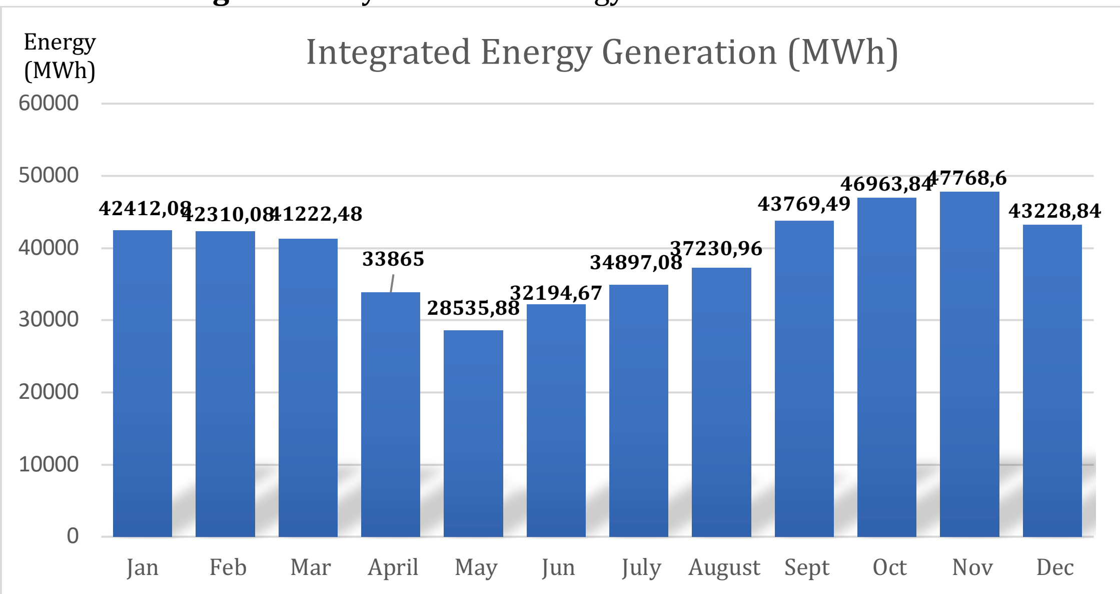

Figure 12. Integrated Energy Generation for each Month

In Figure 12, the integrated energy generation for each month is shown. August records the highest energy generation, primarily due to peak hydropower output. The integration of floating PV significantly enhances overall energy production, particularly in high-output months like November, where total generation increases from 40878.2 MWh to 47768.6 MWh. Conversely, February records the lowest energy generation, reflecting reduced contributions from both hydropower and floating PV during the dry season. However, results show that the minimum hydropower generation in April, initially at 24343 MWh, increases to 33865 MWh with the addition of floating PV. These findings highlight the potential of floating PV integration in stabilizing and improving energy generation throughout the year.

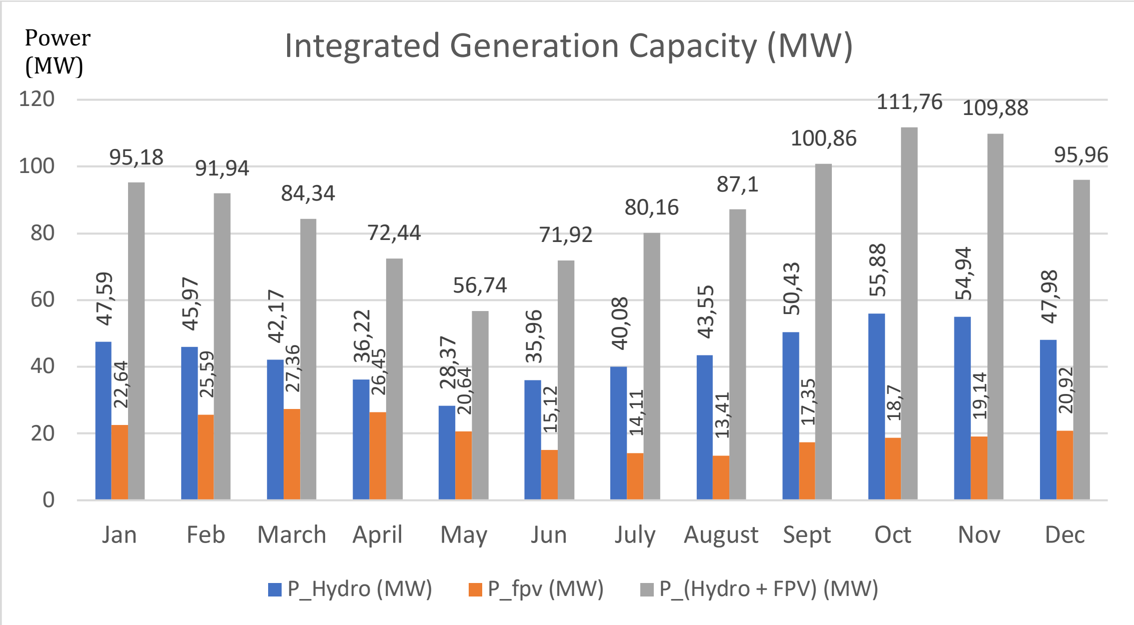

Figure 13. Integrated Generation Capacity for each Month

The integrated capacity of the hydropower system with floating PV is presented in Figure 13. Results indicate that the overall system generation is improved with integration. The standalone hydropower generation does not reach its rated capacity. However, with the inclusion of floating PV, the total system capacity reaches a minimum of 56.74 MW in May and a maximum of 117.68 MW in October.

D. Conclusion

The integration of a floating photovoltaic (PV) system with the Kun Chaung Hydropower Station has been demonstrated to enhance energy generation, optimize resource utilization, and improve overall system capacity. Site assessments have confirmed the reservoir's suitability for floating PV based on factors such as solar irradiance, water levels, and environmental impact. Calculation results indicate a significant increase in energy output, validating the technical feasibility of the integrated system. Results show that the minimum hydropower generation in April, initially at 24343 MWh, increases to 33865 MWh with the addition of floating PV. In November, when hydropower output is at its peak, total generation rises from 40878.2 MWh to 47768.6 MWh. System capacity is also improved, ranging from 56.74 MW in May to 117.68 MW in October. Additionally, floating PV installation is expected to reduce water evaporation rates. To ensure sustained performance, the use of a tilt angle stabilizer is recommended.

This study highlights the benefits of hybridizing floating PV with hydropower and recommends further research to refine performance, develop advanced control strategies, and evaluate economic feasibility. Implementing this system offers a sustainable solution to enhance energy security and expand the renewable energy mix in Myanmar.

E. Acknowledgment

The author is deeply thankful to all of the respectful teachers from Mandalay Technological University, for their instructions, suggestions, and willingness to share their ideas throughout all those years of study and to all persons who helped directly or indirectly towards the successful completion of this paper. Thanks, are also extended to her dear parents for their support and help during this paper and for giving suggestions.

F. References

[1] Al Riza, Dimas Firmanda, and Syed Ihtshamul-Haq Gilani. "Standalone Photovoltaic System Sizing using Peak Sun Hour Method and Evaluation by TRNSYS Simulation." International Journal of Renewable Energy Research (IJRER) 4.1 (2014): 109-114.

[2] Aritra Ghosh. "A comprehensive review of water-based PV: Flotavoltaics, underwater, offshore & canal top." Ocean Engineering 281 (2023) 115044.

[3] Bashria A.A. Yousef, Ali Radwan, Abdul Ghani Olabi, Mohammad Ali Abdelkareem. "Renewable Energy: Solar, Wind, and Hydropower." Elsevier, 2003.

[4] Bouabdallah, A., Bourguet, S., Olivier, J. C., & Machmoum, M. "Photovoltaic energy for the fixed and tracking system based on the modeling of solar radiation." In Industrial Electronics Society, IECON 2013-39th Annual Conference of the IEEE (2013): 1821-1826.

[5] Choi, Y., & Park, H. (2021). "Hybrid Solar and Hydropower Systems: Synergies and Challenges." Energy Systems and Policy, 8(2), 98-110.

[6] Duffie, J. A., & Beckman, W. A. (2013). Solar Engineering of Thermal Processes. Wiley. ISBN: 978-1118095291.

[7] Ficklin, Darren L., et al. "Development and application of a hydroclimatological stream temperature model within the Soil and Water Assessment Tool." Water Resources Research 48.1 (2012).

[8] Fthenakis, V., & Kim, H. C. (2019). "Photovoltaics: Environmental Impacts." In Solar Energy (pp. 245-260). Springer. DOI: 10.1007/978-3-030-29277-7_12.

[9] Gunerhan, H., & Hepbasli, A. (2007). "The Optimal Tilt Angle for Photovoltaic Panels: A Case Study for Turkey." Renewable Energy, 32(14), 2354-2367. DOI: 10.1016/j.renene.2007.02.015.

[10] Hsieh, Bernard B., Johnson, Billy H., & Richards, David R. A Three-Dimensional Numerical Model Study for the Chesapeake and Delaware Canal and Adjacent Bays. WES/TR/HL-93-4.

[11] Hsu, S. A. "Correction of land-based wind data for offshore applications: a further evaluation." Journal of Physical Oceanography, 16.2 (1986): 390-394.

[12] Hsu, Shih-Ang. Coastal meteorology. Elsevier, 2013.

[13] IEA. (2023). World Energy Outlook 2023. International Energy Agency. Retrieved from IEA.

[14] Ishaq, M., Ibrahim, U. H., & Abubakar, H. "Design Of An Off Grid Photovoltaic System: A Case Study Of Government Technical College, Wudil, Kano State." International Journal of Technology Enhancements and Emerging Engineering Research, 2.12 (2013): 175-181.

[15] J. C. N. M. Ng, R. B. M. R. Chia, & M. Y. G. Koh. (2021). "Optimization of Tilt Angle for Photovoltaic Systems in Tropical Climates." Energy Conversion and Management, 234, 113953. DOI: 10.1016/j.enconman.2021.113953.

[16] Kaldellis, J. K., & Zafirakis, D. (2008). "The Role of Tilt Angle in Solar Energy Production for Various Applications." Energy Conversion and Management, 49(12), 3735-3743. DOI: 10.1016/j.enconman.2008.03.022.

[17] Khin, S., & Kyaw, T. (2023). "The Kun Chaung Hydropower Station: A Case Study of Renewable Energy Potential in Myanmar." Energy Resources Journal, 12(4), 145-160.

[18] Masters, Gilbert M. Renewable and Efficient Electric Power Systems. ISBN 0-471-28060-7.

[19] Meteonorm. (2024). Meteonorm Solar Radiation Data. Retrieved from Meteonorm.

[20] Mousazadeh, A., Sharifi, H., Kazemi, H., & Shafieian, S. (2020). "The Impact of Water-Based Cooling on Floating Photovoltaic Systems." Renewable Energy, 146, 2510-2521. DOI: 10.1016/j.renene.2019.08.047.

[21] Nwabuokei, F. I., Awili, C. P. N., & Kwuebene, B. C. I. (2014). "Design of A Stand-Alone Photovoltaic Power System: Case Study of A Residence In Ogwashi-Ukwu, Delta State." Academic Discourse: An International Journal, 7(1), November 2014.

[22] Parmaksiz, Hüseyin, & Karafil, Akif. (2015). "Calculation of optimum fixed tilt angle of PV panels depending on solar angles and comparison of the results with experimental study conducted in summer in Bilecik, Turkey."

[23] REN21. (2023). Renewable Energy Policy Network for the 21st Century. Retrieved from REN21.

[24] Smith, J., & Johnson, L. (2020). "Global Trends in Renewable Energy: The Rise of Solar Power." Renewable Energy Journal, 45(3), 123-135.

[25] Song, J., & Choi, Y. (2016). "Analysis of the Potential for Use of Floating Photovoltaic Systems on Mine Pit Lakes: Case Study at the Ssangyong Open-Pit Limestone Mine in Korea." Energies, 9(2), 102.

[26] Wang, D., & Zhang, T. (2018). "Environmental and Economic Benefits of Integrating Floating Solar with Hydropower." Environmental Science and Technology, 52(9), 5000-5012.

[27] Zhang, Y., & Liu, X. (2019). "Floating Solar Photovoltaic Systems: A Review of Technologies and Applications." Solar Energy, 193, 1-15.